Document downloaded from:

http://hdl.handle.net/10251/187276

This paper must be cited as:

Puche-Panadero, R.; Martinez-Roman, J.; Sapena-Bano, A.; Burriel-Valencia, J.; Pineda-Sanchez, M.; Pérez-Cruz, J.; Riera-Guasp, M. (2021). New Method for Spectral Leakage Reduction in the FFT of Stator Currents: Application to the Diagnosis of Bar Breakages in Cage Motors Working at Very Low Slip. IEEE Transactions on Instrumentation and Measurement. 70:1-11. https://doi.org/10.1109/TIM.2021.3056741

The final publication is available at

https://doi.org/10.1109/TIM.2021.3056741

Copyright Institute of Electrical and Electronics Engineers

Additional Information

New Method for Spectral Leakage Reduction in the FFT of Stator Currents: Application to the Diagnosis of Bar Breakages in Cage Motors Working at Very Low Slip

Ruben Puche-Panadero, *Member, IEEE,*, Javier Martinez-Roman, Angel Sapena-Bano, Jordi Burriel-Valencia, Manuel Pineda-Sanchez, *Member, IEEE*, Juan Perez-Cruz, Martin Riera-Guasp, *Senior Member, IEEE*

***Abstract*—Motor current signature analysis has become a widespread fault diagnosis technique for induction machines, because it is non-invasive, and requires low resources of hardware (a current sensor) and software (a fast Fourier transform). Nevertheless, its industrial application faces practical problems. One of its most challenging scenarios is the detection of broken bars in induction machines working at very low slip, like large machines with a very small rated slip, or unloaded induction motors in off-line tests. In these cases, the leakage of the main supply component can hide the fault harmonics, even with a severe fault. Diverse solutions to this problem have been proposed, such as the use of smoothing windows, advanced spectral estimators, or the removal of the supply component. Nevertheless, these methods modify the spectral content of the current signal or add a high computational burden. In this work, a new approach is proposed, based on the analysis of the current with a very fine spectrum, obtained via simple zero padding, followed by the extraction of a practically leakage-free conventional, coarse spectrum. The method is experimentally validated by the diagnosis of a broken bar fault in a 3.15 MW induction motor.**

***Index Terms*—Condition monitoring, fast Fourier transforms, fault diagnosis, induction machines, spectral leakage.**

I. Introduction

CAGE induction machines (IMs) are a key component of modern industrial processes, due to their robustness and low maintenance requirements. Nevertheless, they can fail, which may cause heavy economical losses due to the unexpected shutdown of complex industrial production lines. Condition based maintenance (CBM) [1] can help reduce this risk by detecting machine faults at an incipient stage [2], [3].

One of the most frequent faults of cage induction machines is the cage winding failure, specially in motors that directly drive high-inertia loads (such as fans), in motors with frequent starts and stops, and in case of poorly manufactured cage windings [4], [5]. This fault must be detected as early as possible, because it can produce heat damage to the rotor core, an increase of the current for a given load, and a reduction of the torque and efficiency [4].

A broken bar fault [6] generates characteristic fault harmonic components [7] in the spectrum of the current, at frequencies f_{bb} given by [8]

$$f_{bb} = f_1(1 \pm 2ks) \qquad k = 1, 2, 3 \ldots, \tag{1}$$

where f_1 is the frequency of the supply component, and s is the slip. Their strength is proportional to the fault severity [9], and is usually expressed as the ratio between the power of the fault harmonic and the supply component, in dB

$$\hat{i}_{dB}(f_{bb}) = 20 \cdot \log_{10}\left(\left|\hat{i}(f_{bb})\right| / \left|\hat{i}(f_1)\right|\right) \tag{2}$$

A value of $\hat{i}_{dB}(f_{bb})$ in (2) greater than -45 dB can be considered as a clear indication of a cage winding fault [4].

In spite of the simplicity of (1) and (2), this method faces practical problems that can make unfeasible its industrial application, solved with the techniques proposed in this work:

- Small errors in the measurement of the frequency f_1 and the amplitude $\hat{i}(f_1)$ of the supply component may produce important errors in the estimation of the position (1) and power (2) of the fault harmonics in the current spectrum.
- At very low slip, the spectral distance between the fault harmonics and the supply component, $f_1 \cdot 2ks$, can be very small [10]. As the supply component dominates the current signal, its spectral leakage at this short distance usually hides completely the fault harmonics [11], of a much lower amplitude (up to 200 times lower [4]).

Therefore, a reliable diagnostic system requires a sharp power spectrum, free of the leakage due to the supply component, with distinguishable peaks at the correct position of the fault harmonics. In the technical literature, this goal has been achieved using different approaches:

- High resolution spectral estimation methods have been proposed using an eigen-based decomposition of the signal current in [12], an spectral estimator based on Rayleigh quotients in [13], Taylor-Kalman filters in cascade with a sub-sampling scheme in [9], or rotational invariance techniques in [14]. In particular, a precise method for measuring the frequency and the amplitude

This work was supported by the Spanish "Ministerio de Ciencia, Innovación y Universidades (MCIU)", the "Agencia Estatal de Investigación (AEI)" and the "Fondo Europeo de Desarrollo Regional (FEDER)" in the framework of the "Proyectos I+D+i - Retos Investigación 2018", project reference RTI2018-102175-B-I00 (MCIU/AEI/FEDER, UE).
The authors are with the Institute for Energy Engineering, Universitat Politècnica de València, Valencia, Spain (e-mail: rupucpa@die.upv.es, jmroman@die.upv.es, asapena@die.upv.es, jorburva@die.upv.es, mpineda@die.upv.es, juperez@die.upv.es, mriera@die.upv.es).

of the supply component with high accuracy using spectral interpolation with the amplitudes of the largest two spectral components bins has been presented in [15]. This approach was termed as the interpolated FFT (IFFT) in [16]. In [17], [18] a three-point interpolation schema is proposed to reduce the amplitude error about ten times compared with the usual one-point method, and in [19] it has been expanded to a nine-point method, which decreases systematic errors but increases noise distortion. An iterative weighted phase averager (IWPA) has been presented in [20], which can even distinguish sinusoids with a frequency separation smaller than the periodogram's resolution limit. Nevertheless, this approach requires a new iteration to obtain each new component as the strongest peak of the remaining residual and then to re-estimate the parameters of all the previously obtained components.

- Regarding the reduction of the spectral leakage, the classical method consists in windowing the current signal with a weighting window [21], [22], such as the Hanning window [23], [24], the Hamming window [25], and many others window types. Compared with the rectangular window, the default one when sampling the current signal during a limited acquisition time, other weighting windows reduce the side lobe levels, thus improving the detectability of weak frequency components. Nevertheless, those windows also reduce the signal-to-noise ratio (SNR) relative to the SNR of the default rectangle window [21]. Moreover, a window with a very narrow main lobe has a high spectral resolvability. In this regard, the default rectangle window has the narrowest main lobe, equal to the periodogram's resolution limit. Some authors propose alternatives solutions to the leakage problem such as reducing the fundamental component of the current [26], filtering it, using notch filters [27] and Kalman filters [28], or rectifying the current signal [29].

Nevertheless, the aforementioned solutions depart from the simplicity of the basic FFT-based approach. Interpolated FFTs requires a greater computational effort, which depend on the number samples used for performing the interpolation procedure, and also on the number of iterations required, as in IWPA. On the other hand, the use of weighting windows different than the rectangular one reduce the SNR, increase the frequency measurement uncertainty due to their wider main lobe, and may distort the spectrum of the original current signal, being a low pass filter in the frequency domain. For example, the Hanning window doubles the base width of the peaks of the fault harmonics, hampering their accurate detection.

On the contrary, the novel method proposed in this work uses only the Fourier transform as the signal processing technique, with the default rectangular window to maximize the spectral resolvability, and does not alter the spectral content of the current signal. The problem of the high side lobe levels of the rectangular window is solved by carefully aligning the periodogram bins with the zeros of these side lobes. The proposed approach is based on the calculation of a fine spectrum of the zero-padded sampled current, followed by the extraction of a leakage-free coarse spectrum, what allows the detection of very small fault harmonics close to the fundamental.

The structure of the paper is as follows: in Section II the spectral leakage issue is analyzed, and in Section III, it is evaluated for the case of a broken bar fault. Section IV presents the proposed method, and in Section V it is validated by applying it to a large industrial motor with a low rated slip, and compared with the results obtained by interpolating the FFT bins and using weighting windows. Finally, Section VI presents the conclusions of this work.

II. Spectral Leakage in the Current Spectrum

In this section, the problem of the spectral leakage of the supply component of the machine current is analyzed. For simplicity, in this section an ideal IM is considered, with a stator current that only contains the supply component and the principal fault harmonic components, $k = \pm 1$ in (1), that is

$$i(t) = I\cos\big(2\pi f_1 t\big) + \beta I\cos\big(2\pi f_1(1 \pm 2s)t\big) \tag{3}$$

where β indicates the severity of the fault ($\beta \ll 1$).

A. Continuous Fourier Transform (CFT) of the Infinite-Length Current Signal of an Ideal IM

The current $i(t)$ in (3) is an infinite-length time signal which spans from $t = -\infty$ to $t = \infty$. Its CFT, $\hat{i}(f)$, is given by

$$\mathrm{CFT}\big(i(t)\big) = \hat{i}(f) = \int_{-\infty}^{\infty} i(t)e^{-i2\pi ft}dt \tag{4}$$

which, applied to (3), gives

$$\begin{aligned}\hat{i}(f) = \frac{I}{2}\delta(f - f_1) + \beta\frac{I}{2}\big(\delta(f - f_1(1 \pm 2s)\big) + \\ + \frac{I}{2}\delta(f + f_1) + \beta\frac{I}{2}\big(\delta(f + f_1(1 \pm 2s)\big)\end{aligned} \tag{5}$$

where δ is the Kronecker delta function. As the transform of a real signal exhibits Hermetian symmetry, $\hat{i}(f) = \hat{i}^*(-f)$ [21], only the positive frequencies of the current spectrum will be considered from now on. Also, it will be assumed that the supply frequency f_1 is far enough from the origin ($f = 0$) so that the leakage coming from the negative part of the spectrum can be neglected. Therefore, (5) becomes

$$\hat{i}(f) = \frac{I}{2}\delta(f - f_1) + \beta\frac{I}{2}\delta\big(f - f_1(1 \pm 2s)\big). \tag{6}$$

Equation (6) constitutes the characteristic signature of a broken bar fault: a spectral component at the frequency of the supply component f_1, and two sideband harmonics, at frequencies given by (1), with a much lower amplitude. The stator current signal of an ideal machine with a broken bar fault $i(t)$ and its CFT, $\hat{i}(f)$, given in (5) and (6), taking $\beta = 0.02$, are plotted in Fig. 1.

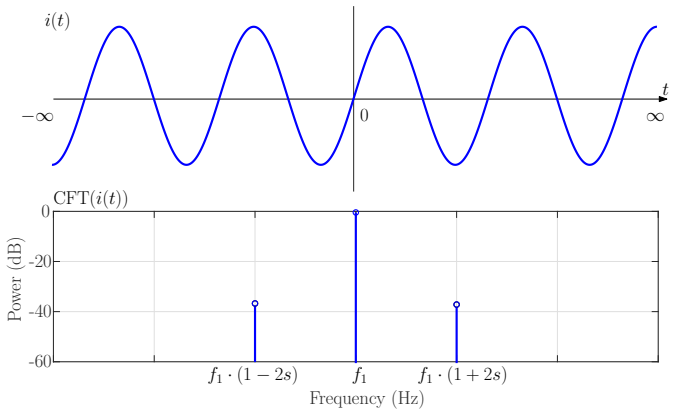

Fig. 1. Infinite-length stator current of an ideal induction motor with broken bars (top), and its CFT (bottom) for a parameter $\beta = 0.02$ in (5) and (6), showing the characteristic sideband harmonics at frequencies (1) as Kronecker deltas in the frequency domain.

B. CFT of the Measurable Current Signal of an Ideal IM

In the real world it is not possible to get a signal $i(t)$ of infinite duration. The diagnostic task has to be carried out from measurable currents $i_m(t)$ that can be captured during a restricted acquisition time, T_{acq}. Thus, the starting point for the fault diagnosis process is the measurable current, a continuous function restricted to a specific time interval, defined as

$$i_m(t) = i(t) \quad t \in [0, T_{acq}] \tag{7}$$

Nevertheless, for calculating the CFT of $i_m(t)$, it is necessary to define it in the interval $-\infty < t < \infty$; for this reason, it is advisable to introduce the time-expanded measurable current $i_{me}(t)$, which is defined as (see Fig. 2, top)

$$i_{me}(t) = \begin{cases} 0 & -\infty < t < 0 \\ i(t) & 0 \leq t \leq T_{acq} \\ 0 & T_{acq} < t < \infty \end{cases} \tag{8}$$

In this way, a CFT can be associated to the time-restricted signal $i_m(t)$, as the CFT of $i_{me}(t)$

$$\text{CFT}\big(i_{me}(t)\big) = \hat{i}_{me}(f) = \int_{-\infty}^{\infty} i_{me}(t) e^{-i2\pi ft} dt \tag{9}$$

On the other hand, $i_{me}(t)$ can be also defined as the product of the infinite duration current signal $i(t)$ and a rectangular window of unit height and duration T_{acq}, $\text{rect}_{T_{acq}}(t)$

$$i_{me}(t) = i(t) \cdot \text{rect}_{T_{acq}}(t) \tag{10}$$

As $i_{me}(t)$ is the product of two functions in the time domain (10), its CFT is the convolution ($*$) in the frequency domain of the CFTs of these two functions,

$$\text{CFT}\big(i_{me}(t)\big) = \text{CFT}\big(i(t)\big) * \text{CFT}\big(\text{rect}_{T_{acq}}(t)\big) \tag{11}$$

The CFT of the rectangular window is the sinc function,

$$\text{CFT}\big(\text{rect}_{T_{acq}}(t)\big) = \text{sinc}(f \cdot T_{acq}) = \frac{\sin(\pi f \cdot T_{acq})}{\pi f \cdot T_{acq}} \tag{12}$$

Replacing (6) and (12) in (11) gives the CFT of the time-expanded measurable current signal, $\hat{i}_{me}(f)$,

$$\begin{aligned} \hat{i}_{me}(f) \approx \frac{I}{2}\text{sinc}\Big(\big(f - f_1\big) \cdot T_{acq}\Big) + \\ + \beta\frac{I}{2}\text{sinc}\Big(\big(f - f_1(1 \pm 2s)\big) \cdot T_{acq}\Big) \end{aligned} \tag{13}$$

The time-expanded measurable current signal of a machine with a broken bar fault $i_{me}(t)$ and its CFT (13) (in dB, $\beta = 0.02$) are represented in Fig. 2, showing the characteristic sidelobes generated by the rectangular time window, with a width $\Delta f = 1/T_{acq}$. It should be noted that, in the spectrum of Fig. 2, besides the expected harmonics at frequencies f_1, $f_1(1-2s)$ and $f_1(1+2s)$, the CFT has non-zero amplitude at every other frequency, due to the finite acquisition time T_{acq}. It is also worth mentioning that the rectangular time window is the one with the narrowest main lobe for a given acquisition time.

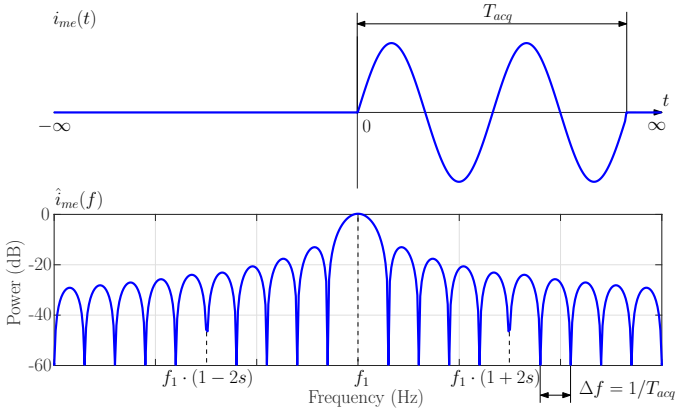

Fig. 2. Time-expanded measurable stator current $i_{me}(t)$ of an ideal induction motor with broken bars ($\beta = 0.02$), obtained during an acquisition time T_{acq} (top), and its CFT (bottom), with the characteristic sidelobes produced by the finite acquisition time. The current signal has infinite length, with a zero value outside the rectangular time window of length T_{acq}.

C. Fine Discrete Fourier Transform of the Current Signal

In practical applications, the stator current is sampled during a time T_{acq}, at a rate f_s. This generates a discrete sequence of $N = T_{acq} \cdot f_s$ samples, $i_s[n]$, $n = 0, \ldots, N-1$, whose spectrum has N frequency bins, with a separation given by the width of the lobes of the rectangular time window of Fig. 2,

$$\Delta f = f_s/N = 1/T_{acq} \tag{14}$$

As in (8), a time-expanded sampled signal $i_{se}[n]$ can be defined by zero-padding the original signal $i_s[n]$, of N elements, giving a new sequence of $N' >> N$ elements $i_{se}[n]$, as

$$i_{se}[n] = \begin{cases} i_s[n] & n = 0, \ldots, N-1 \\ 0 & n = N, \ldots, N'-1 \end{cases} \tag{15}$$

The $i_{se}[n]$ signal is a better approximation to the time-expanded measurable current $i_{me}(t)$ (continuous signal) than the raw sampled signal $i_s[n]$. Its discrete Fourier transform (DFT) is given by

$$\hat{i}_{se}[k] = \sum_{n=0}^{N'-1} i_{se}[n] \cdot e^{-\frac{2\pi i}{N'}kn} \quad k = 0, \ldots, N'-1 \tag{16}$$

As N' increases, the separation between the frequency bins in the DFT spectrum of $i_{se}[n]$ decreases, and tends to the continuous CFT spectrum of $i_{me}(t)$, so (16) can be considered as a fine DFT (fDFT) associated to the sampled signal $i_s[n]$; it is not the continuous CFT of $i_{me}(t)$ in (13), but a finite set of N' bins corresponding to a fine sampling approximation of the CFT at the points $k \cdot \Delta f' = k \cdot f_s/N'$, $k = 0, \ldots, N'-1$. That is

$$\begin{aligned} \text{fDFT}\big(i_s[n]\big) = \hat{i}_{se}[k] \approx \text{CFT}\big(i_{me}(t)\big)\Big|_{f=(k\Delta f')} = \\ = \hat{i}_{me}(k \cdot \Delta f') \qquad k = 0, \ldots, N'-1 \end{aligned} \tag{17}$$

Taking into account (14) and (13), finally (17) becomes

$$\begin{aligned} \text{fDFT}\big(i_s[n]\big) = \hat{i}_{se}[k] \approx \frac{I}{2}\text{sinc}\Big(\big(k\Delta f' - f_1\big)/\Delta f\Big) + \\ + \beta\frac{I}{2}\text{sinc}\Big(\big(k\Delta f' - f_1(1 \pm 2s)\big)/\Delta f\Big) \qquad k = 0, \ldots, N'-1 \end{aligned} \tag{18}$$

as represented in Fig. 3.

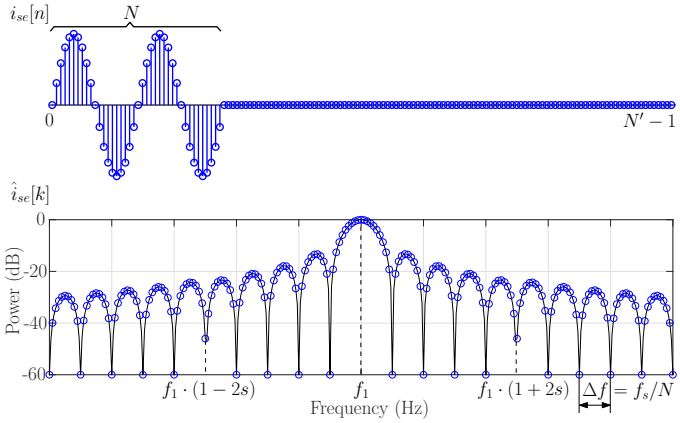

Fig. 3. Time-expanded sampled stator current $i_{se}[n]$ of an ideal induction motor with broken bars ($\beta = 0.02$) zero-padded up to N' elements, (top), and its corresponding fDFT (blue circles, bottom). The fDFT samples the CFT of $i_{me}(t)$ (thin, black, line bottom) at points separated $\Delta f' = f_s/N'$.

D. Conventional, coarse DFT of the Current Signal

Usually, the DFT of the sampled current signal is built using only the N samples obtained during the acquisition time, T_{acq}, without zero padding, that is,

$$\hat{i}_s[k] = \sum_{n=0}^{N-1} i_s[n] \cdot e^{-\frac{2\pi i}{N}kn} \quad k = 0, \ldots, N-1 \tag{19}$$

This choice leads in fact to generate the coarsest spectrum for a given acquisition time, with a distance between frequency bins equal to Δf (14). Therefore, the conventional, coarse DFT (cDFT) of $i_s[n]$ consists of a finite set of N bins calculated through (19), corresponding to a coarse sampling approximation of the CFT of $i_{me}(t)$ at the points $k \cdot \Delta f = k \cdot f_s/N$, $k = 0, \ldots, N-1$. That is

$$\begin{aligned} \text{cDFT}\big(i_s[n]\big)\big) = \hat{i}_s[k] \approx \text{CFT}\big(i_{me}(t)\big)\Big|_{f=(k\Delta f)} = \\ = \hat{i}_{me}(k \cdot \Delta f) \qquad k = 0, \ldots, N-1 \end{aligned} \tag{20}$$

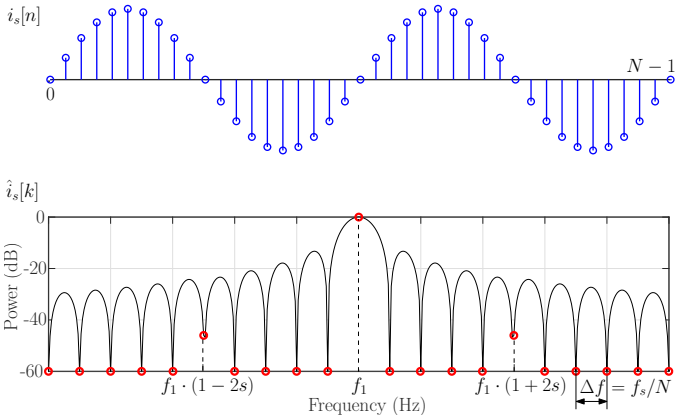

Fig. 4. Sampled stator current $i_s[n]$ of an ideal induction motor with broken bars (N elements, no zero-padding $\beta = 0.02$) (top), and its corresponding conventional cDFT (red circles, bottom). The cDFT samples the continuous CFT of $i_{me}(t)$ (thin, black line, bottom) at points separated $\Delta f = f_s/N$. This choice gives only one sample per sidelobe of the CFT, the coarsest possible spectrum for a given acquisition time. The supply frequency lies on a bin of the cDFT in this example.

Taking into account (13) and (14), finally (20) becomes

$$\begin{aligned} \text{cDFT}\big(i_s[n]\big)\big) = \hat{i}_s[k] \approx \frac{I}{2}\text{sinc}\Big(k - f_1/\Delta f\Big) + \\ + \beta\frac{I}{2}\text{sinc}\Big(k - f_1 \cdot (1 \pm 2s)/\Delta f\Big) \qquad k = 0, \ldots, N-1 \end{aligned} \tag{21}$$

This expression of the conventional cDFT can also be deduced by setting $\Delta f' = \Delta f$ in (18).

From (21), it follows that the cDFT samples the CFT of $i_{me}(t)$ at a single point per lobe of the rectangular time window (see Fig. 4). Therefore, it can be considered a coarse subset of the fDFT. Fig. 5 shows graphically the relationship between (13), (18) and (21). From a diagnostic point of view, it is clear that the fault harmonics are better identified in the cDFT spectrum (Fig. 5, red line) than in the finer fDFTspectrum (Fig. 5, blue circles). Nevertheless, this is only true if the cDFT bins are chosen as the fDFT bins with the minimum leakage, as proposed in this paper.

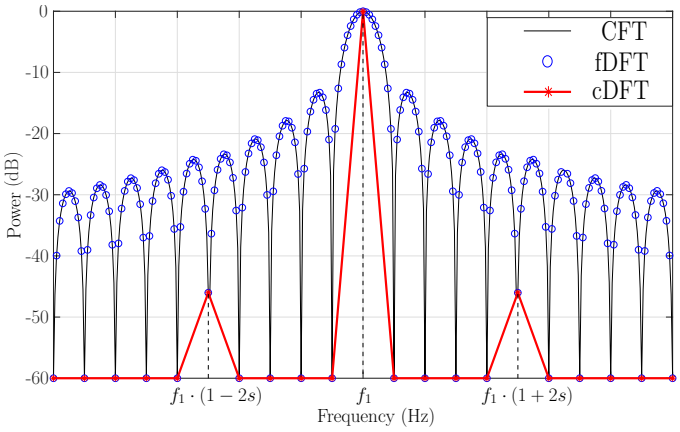

Fig. 5. Comparison between the CFT of the stator current of a faulty machine (thin, black line), its fDFT (blue circles) and its cDFT (thick, red line). The supply frequency coincides with a bin of the cDFT in this example.

III. Quantification of the Spectral Leakage

As shown in Section II, in the case of a current signal measured during a finite acquisition time T_{acq}, the harmonic components of the current are no longer represented in its spectrum by peaks (Kronecker delta functions). Instead, each component gives rise to a function with defined values for all frequencies. This effect, the spectral leakage, is especially important in the case of the supply component, since its amplitude in the current signals used in fault diagnosis is usually two orders of magnitude greater than the rest of the harmonic components.

The first term of (13) reflects the effect of the supply component on the harmonic amplitude at every frequency of the CFT spectrum. Therefore, it is denoted as $\hat{i}_{me}(f)\big|_{fund}$, and gives the theoretical expression of the leakage as

$$\hat{i}_{me}(f)\big|_{fund} \approx \frac{I}{2}\text{sinc}\left(\frac{f-f_1}{\Delta f}\right) \tag{22}$$

Fig. 6 plots the modulus of (22), in dB, in the proximity of the supply frequency (50 Hz). From (22), and observing Fig. 6, the following properties of the leakage can be deduced:

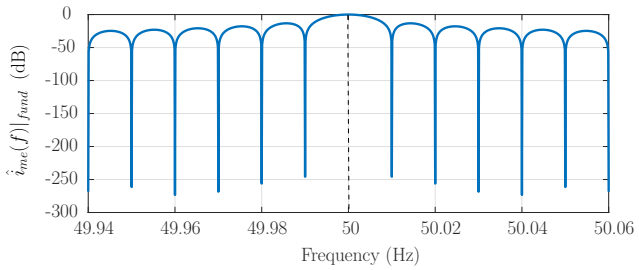

Fig. 6. Modulus of the theoretical spectral leakage (22) produced by the supply component in its proximity.

- The leakage function (22) evolves cyclically, describing sidelobes around the supply frequency, of width $\Delta f = 1/T_{acq}$. It presents steep changes, of more than 250 dB in a extremely narrow frequency interval around its minima, as seen in Fig. 6.
- For a given frequency f, the leakage depends on the argument of the sinc function in (22), that is, the distance between f and the supply frequency f_1, expressed as a multiple of the width Δf of the sidelobes.
- There is a reduced set f_{0z} of leakage free frequencies, corresponding to the minima in Fig. 6, whose distance to the supply frequency is an integer multiple of the lobe width ($f_{0z} - f_1 = k_z \cdot \Delta f$, with $k_z \in \mathbb{Z}$), thus making null (22).
- For the rest of frequencies, $f - f_1 = d_f \cdot \Delta f$, with $d_f \notin \mathbb{Z}$, the leakage depends mainly on the fractional part of d_f, rather than its total value (in the proximity of the supply frequency). For example, with a distance between frequency bins $\Delta f = 0.1$ Hz, ($T_{acq} = 10$ s), the leakage is mainly determined by the hundredths of Hz in $(f - f_1)$; if $\Delta f = 0.01$ Hz, ($T_{acq} = 100$ s), which is relevant are the thousandths of Hz in $(f - f_1)$.

A. The Picket Fence Error

The frequencies of the bins of the cDFT are given by $f_k = k \cdot \Delta f$, $k = 0, \ldots, N-1$. However, it is very unlikely that the frequencies of the supply component f_1 and of the fault harmonics f_{bb} (2) exactly match any of the frequencies f_k. Therefore, they are approximated by the nearest discrete frequencies $f_{1\_app} = k_1 \Delta f$ and $f_{bb\_app} = k_{bb} \Delta f$, respectively, which may lead to errors (picket fence errors) in the estimation of the amplitudes and frequencies of the analyzed components.

B. Oscillations of the Network Frequency

In large electrical systems in quasi stationary functioning, a frequency error is inherent and necessary for self regulation of the system. The system frequency oscillates in a range of ± 150 mHz around the rated frequency, and depends on the deviation of the predicted demand against the actual one, which varies randomly. The deviation between the actual value of the supply frequency and its assumed value (equal to the rated mains frequency f_{1r}), when calculating the current spectrum by means of the cDFT, determines the appearance of picket fence and leakage errors, which frequently make the diagnosis unfeasible. Fig. 5 shows an ideal case in which $f_1 \equiv f_{1r} = 50$ Hz. In these conditions the supply frequency exactly matches one of the cDFT bins, thus its measured amplitude exactly matches the actual one (no picket fence error). In addition, the rest of the cDFT bins are separated from the supply frequency by an integer number of lobes. Therefore, they are not affected by its leakage, the resulting cDFT spectrum is very clear (red line), and the characteristic peaks of the fault harmonics are clearly discernible. On the contrary, Fig. 7 has been obtained by imposing a deviation of the supply frequency of just 5 mHz ($f_1 = 50.005$ Hz). In this case, the leakage of the supply component is much bigger than the amplitude of the fault harmonics, which makes them undetectable (misdiagnosis).

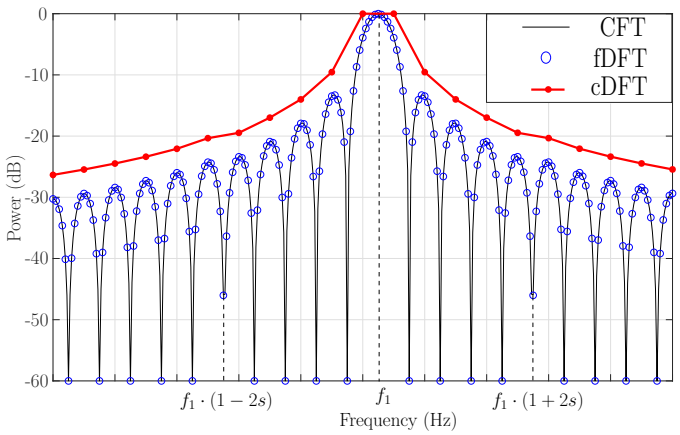

Fig. 7. Comparison between the CFT of the stator current of a faulty machine (thin, black line), its fDFT (blue circles), and its conventional cDFT (thick, red line). The supply frequency lies in the middle of two bins of the conventional cDFT in this example.

IV. Proposed Method for the Reduction of the Leakage in the Current Spectrum

The first term of (18), which will be designated as $\hat{i}_{se}[k]\big|_{fund}$ as in (22), is the theoretical value of the leakage produced by the supply component at each k bin of the fDFT,

$$\hat{i}_{se}[k]\big|_{fund} \approx \frac{I}{2}\text{sinc}\Big((k\Delta f' - f_1)/\Delta f\Big) \quad k = 0, \ldots, N'-1 \tag{23}$$

The maximum picket fence errors in the frequency and in the amplitude of the supply component occurs when its actual frequency lies in the middle of two fDFT bins ($f_1 = k_1\Delta f' \pm \Delta f'/2$), as shown in Fig. 7. In this case,

- the maximum frequency error, $\epsilon_{1f,max}$, is given by

$$\epsilon_{1f,max} = (k_1\Delta f' - f_1) = \frac{\Delta f'}{2} \tag{24}$$

- the maximum amplitude error, $\epsilon_{1A,max}$, is given by

$$\begin{aligned}\epsilon_{1A,max} =& \hat{i}[f_1] - \hat{i}_{se}[k]\big|_{fund} \approx \\ \approx& \frac{I}{2} - \frac{I}{2}\text{sinc}\Big((k_1\Delta f' - f_1)/\Delta f\Big) = \\ =& \frac{I}{2}\Big(1 - \text{sinc}\Big(\Delta f'/2\Delta f\Big)\Big)\end{aligned} \tag{25}$$

For comparison purposes, it is convenient to introduce the padding ratio R_N as the ratio between the number of samples used in the fDFT (N') and in the cDFT (N),

$$R_N = N'/N = (f_s/N)/(f_s/N') = \Delta f/\Delta f' \tag{26}$$

Thus, substituting (26) in (24) and (25), the maximum picket fence errors of the supply component, in frequency (Hz) and amplitude (in % of its actual value), are

$$\begin{aligned}\epsilon_{1f,max} &= \frac{\Delta f}{2R_N} \\ \epsilon_{1A,max,\%} &\approx 100\,\Big(1 - \text{sinc}\Big(\frac{1}{2R_N}\Big)\Big)\end{aligned} \tag{27}$$

Expression (27) shows that the maximum errors in frequency and amplitude are inversely proportional to the padding ratio R_N. The cDFT ($R_N = 1$) has a maximum amplitude error (see Fig. 8) of 36.34%, while the fDFT, with the padding ratio $R_N = N'/N = 10$ used in this work, has a maximum error of only 0.41%, a 100-fold error reduction. From Fig. 8 it is justified that the use of padding ratios greater than 10 does not introduce appreciable improvements in the reduction of the amplitude error.

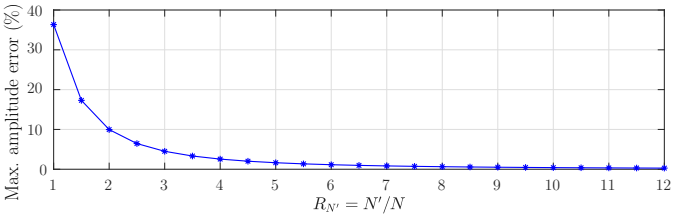

Fig. 8. Maximum value of the amplitude error, which occurs when the actual supply frequency lies in the middle of two DFT bins, as a function of the padding ratio R_N. It can be reduced from 36.34% in the cDFT to 0.41% in the fDFT, with the padding ratio $R_N = 10$ used in this work.

A. Reduced Leakage Spectrum Extracted from the fDFT

To present the process of generating the reduced leakage spectrum of the current signal proposed in this work, a particular case has been represented in Fig. 9, in which the actual supply frequency, $f_1 = 50.033$ Hz, does not match exactly its rated value $f_{1r} = 50$ Hz ($f_1 \neq f_{1r}$). The solid black line in Fig. 9, top, represents the function $\hat{i}_{me}(f)\big|_{fund}$. Superimposed on this graph, the function $\hat{i}_{se}[k]\big|_{fund}$ is plotted (small black circles), showing the leakage of the supply component. The highlighted circles mark the bins of the cDFT of the sampled current ($\hat{i}_s[k]$). The largest one coincides with the rated frequency, f_{1r}, which does not exactly match its actual value f_1, in this example.

As discussed in Section III, the function $\hat{i}_{me}(f)\big|_{fund}$ is null at frequencies f_{0z} whose distance to f_1 is an integer multiple of Δf; these frequencies are given by the condition

$$\begin{aligned}\hat{i}_{me}(f)\big|_{fund} = 0 \rightarrow \frac{f_{0z} - f_1}{\Delta f} = k_z \rightarrow \\ \rightarrow f_{0z} = f_1 + k_z \cdot \Delta f \quad k_z \in \mathbb{Z}\end{aligned} \tag{28}$$

Therefore, in the spectrum of $\hat{i}_{me}(f)$, the bins at frequencies $f_{0z} = f_1 + k_z \cdot \Delta f$ are free of leakage. Unfortunately, it is highly unlikely that the spectrum $\hat{i}_{se}[k]$ of an actual sampled signal contains the set of bins placed exactly at frequencies f_{0z}, due to the shape of the leakage function (Fig. 6). In this case, all the bins will be affected by the leakage of the supply component, specially in its proximity.

However, it is always possible to select a set of N bins separated each other Δf Hz, with the minimum achievable leakage for a given signal and padding ratio R_N. This set, that will be designated as 'reduced leakage DFT' (RLDFT), consists of the fDFT bins that are closest to the frequencies f_{0z} (highlighted red circles in Fig. 9, bottom). The bin corresponding to the supply component (at a frequency $k_1 \cdot \Delta f'$ in Fig. 9, bottom) belongs to this set, and can be easily identified as the dominant peak in the fDFT spectrum. The remaining bins of the RLDFT are simply those separated from it a frequency equal to integer multiples of Δf (28), as

$$\begin{aligned}k_{0z} \cdot \Delta f' = k_1 \cdot \Delta f' + k_z \cdot \Delta f \rightarrow k_{0z} = k_1 + k_z \cdot R_N \\ 0 < k_{0z} \leq N,\ k_z \in \mathbb{Z}\end{aligned} \tag{29}$$

The coefficients k_{0z} can be calculated more easily as

$$k_{0z} = m + z \quad z = 0, \ldots, N-1 \tag{30}$$

where

$$m = k_1 - R_N \cdot \text{floor}(k_1/R_N) \tag{31}$$

As shown in Fig. 9, m represents the offset of the RLDFT bins with respect to those of the conventional cDFT. In this case, an offset of just $m = 3$ bins leads to a 60 dB reduction of the leakage error.

B. Practical Application Scheme of the Proposed Approach

The steps for the practical application of the proposed method for reducing the supply component leakage are:

1) Sampling the stator current, $i_m(t)$, during an acquisition time T_{acq}, at a rate f_s. This produces a sequence of

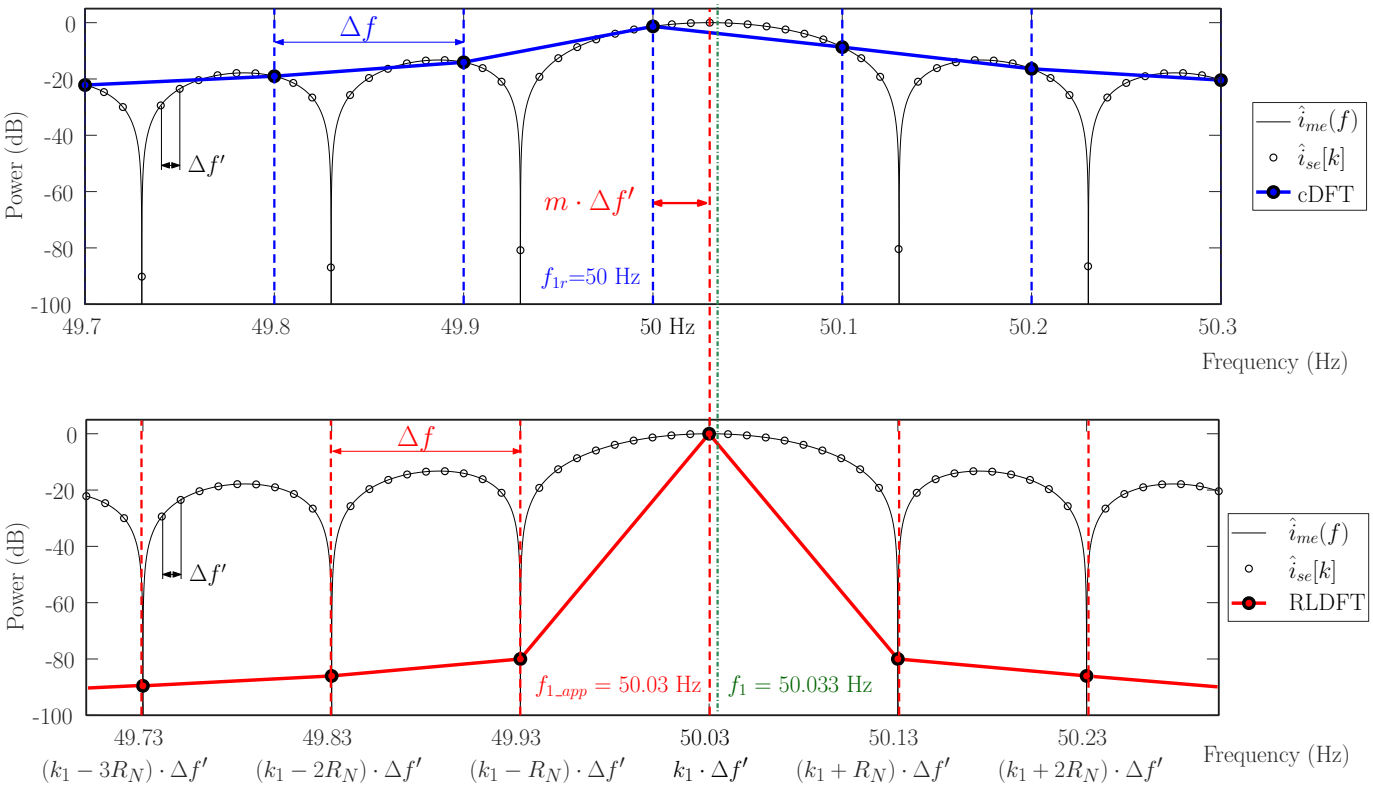

Fig. 9. Leakage amplitude in the generic case in which the actual supply frequency (f_1=50.033 Hz) does not exactly match its rated value (f_{1r}=50 Hz). The highlighted circles in the top figure correspond to the conventional cDFT, with a separation between frequency bins Δf = 0.1 Hz. The highlighted red circles in the bottom plot indicate the bins of the fDFT in which the leakage is minimal, that is, the RLDFT bins. They have the same frequency separation as the cDFT, Δf, but with a much lower leakage. In the case represented in this figure, $R_N = 10$ and $m = 3$, reaching the RLDFT a reduction of the supply spectral leakage of more than 60 dB regarding the conventional cDFT. Besides, the actual supply frequency is better approximated by the fDFT, with a value of $f_{1\_app} = 50.03$ Hz, than by the cDFT, whose maximum peak is found at 50 Hz.

$N = T_{acq} \cdot f_s$ samples, $i_s[n]$ ($n = 0, \ldots, N-1$), with a separation between frequency bins of $\Delta f = 1/T_{acq} = f_s/N$ Hz.

2) Obtaining the time-expanded sampled signal by zero padding the sampled signal as

$$i_{se}[n] = \begin{cases} i_s[n] & n = 0, \ldots, N-1 \\ 0 & n = N, \ldots, N'-1 \end{cases} \tag{32}$$

From a practical point of view, it is convenient to choose a padding ratio R_N first and then calculate $N' = N \cdot R_N$. Increasing R_N allows to reduce leakage more, but increases the computational cost. In this work a ratio $R_N = 10$ is chosen ($N' = 5 \cdot 10^6$ samples).

3) Calculating the fDFT of $i_s[n]$, as the DFT of $i_{se}[n]$ (fDFT$(i_s[n]) = \hat{i}_{se}[k]$). Once N' is set, the separation between frequency bins is $\Delta f' = f_s/N' = \Delta f/R_N$ Hz.

4) Obtaining the best approximation to the frequency of the main supply component, f_{1_app}, as the frequency of the bin with the maximum amplitude in the fDFT spectrum, at index

$$k_1 = f_{1\_app}/\Delta f' \tag{33}$$

5) Calculating the parameter m, using (33) in (31).

6) Obtaining the RLDFT corresponding to the sampled signal $i_s[n]$. It is built by selecting N elements of $\hat{i}_{se}[k]$, separated each other by R_N elements, and starting from the element with index m

$$\text{RLDFT}(i_s[n]) = \hat{i}_{se}[m + k \cdot R_N] \qquad k = 0, \ldots, N-1 \tag{34}$$

The RLDFT (34) is as coarse as the cDFT (20), having the same separation between their frequency bins. Nevertheless, the new set of the RLDFT bins, at frequencies

$$f_{k_{0z}} = \left(m + k \cdot R_N\right) \cdot \Delta f' \qquad k = 0, \ldots, N-1 \tag{35}$$

have been shifted the exact amount $m \cdot \Delta f'$ needed to achieve the minimum leakage for a given sampled current signal $i_s[n]$ and for a given padding ratio R_N.

V. Experimental validation

The proposed method has been applied to the diagnosis of a broken bar fault in a large 3.15 MW motor (Appendix A), and confirmed by a visual inspection of the rotor. The motor current has been sampled at a rate $f_s = 5$ kHz during an acquisition time $T_{acq} = 100$ s, with a distance between frequency bins of $\Delta f = 0.01$ Hz. The measured motor slip is $s = 0.0018$, and the power spectrum of the current signal, Fig. 10, obtained with the conventional cDFT, shows the supply component at 49.98 Hz. Substituting these values in (1), the expected frequencies of the fault harmonics are 49.80 Hz and 50.16 Hz, for $k = \pm 1$, and 49.62 Hz and 50.24 Hz, for

$k = \pm 2$. Nevertheless, due to the leakage of the fundamental, there are no visible peaks in the spectrum at these frequencies, in spite of such a long acquisition time (misdiagnosis).

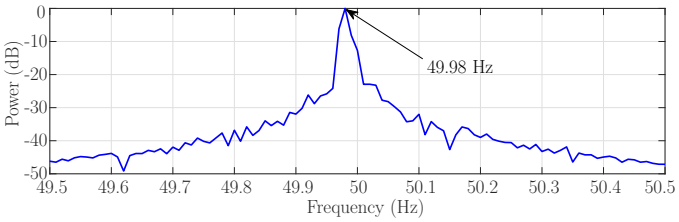

Fig. 10. Power spectrum of the stator current of the faulty machine, with a broken bar fault. Due to the leakage of the supply component, the fault harmonics, expected at 49.62 Hz, 49.80 Hz, 50.16 Hz and 50.24 Hz, are not visible.

In Fig. 11 the reasons of this misdiagnosis are revealed using the fDFT, obtained with a padding ratio $R_N = 10$:

- The cDFT bins have been calculated at frequencies with a significant leakage of the fundamental.
- The frequency (49.98 Hz) and the amplitude of the highest peak in the cDFT spectrum are far from the actual values of the supply component.

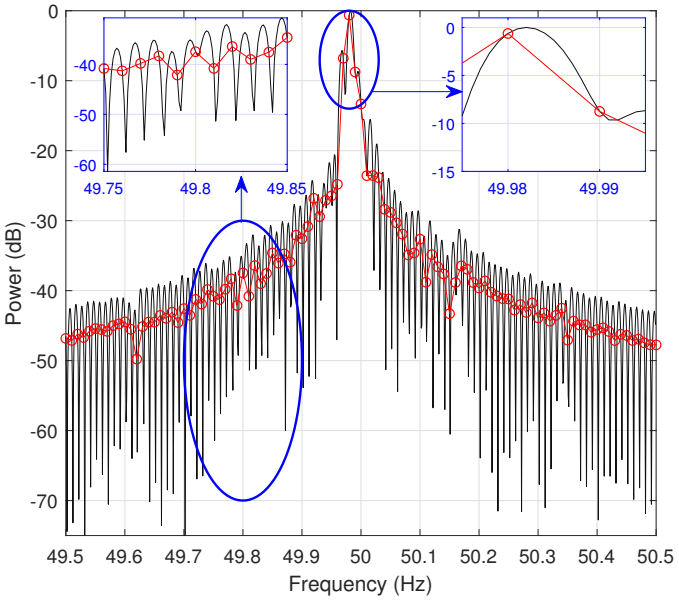

Fig. 11. CFT of the current of the faulty machine (thin, black line), and conventional cDFT of the current (red circles). As the cDFT, in this case, samples the CFT at points where the sidelobes are not minimum, the leakage completely hides the fault harmonics.

In Fig. 12, the proposed method to solve these problems is depicted. The frequency of the supply component, measured in the fDFT (thin, black line), is $f_{1\_app} = 49.982$ Hz, with a maximum error less than 0.41%, regarding its exact, unknown value (see Section IV). Following the steps 4-6 of Section IV-B, the RLDFT is built (red circles in Fig. 12), by selecting the bins of the fDFT whose distance from f_{1_app} is an integer multiple of the lobe width $\Delta f = 0.01$ Hz.

Fig. 13 shows the final result. In the RLDFT (red line), unlike in the conventional cDFT (blue line), the fault harmonics are clearly visible, their frequencies agree with the theoretical

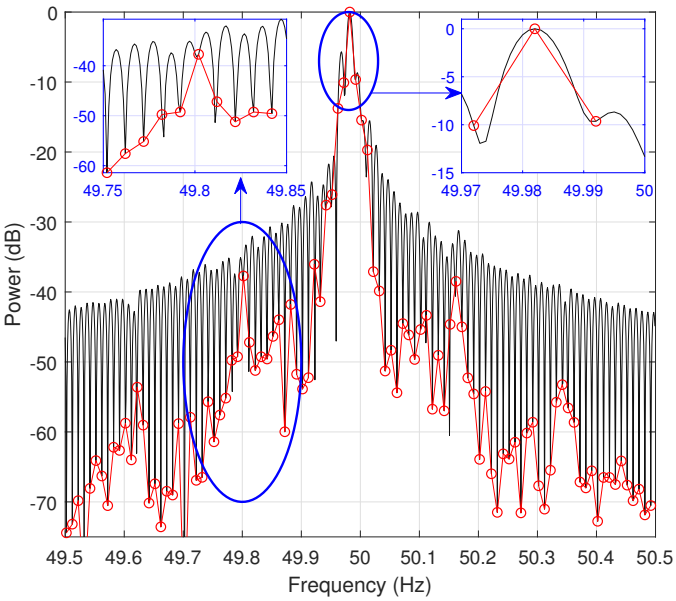

Fig. 12. CFT of the stator current of the faulty machine (thin, black line), and RLDFT of the current signal (red circles). The RLDFT samples the CFT of $i_{me}(t)$ at points where the leakage of the supply component is minimum.

ones (1) up to the mHz, and their amplitudes (for $k = \pm 1$) are greater than -45dB (-37.73 dB), which is an indication of a broken bar fault [4], thus avoiding the misdiagnosis.

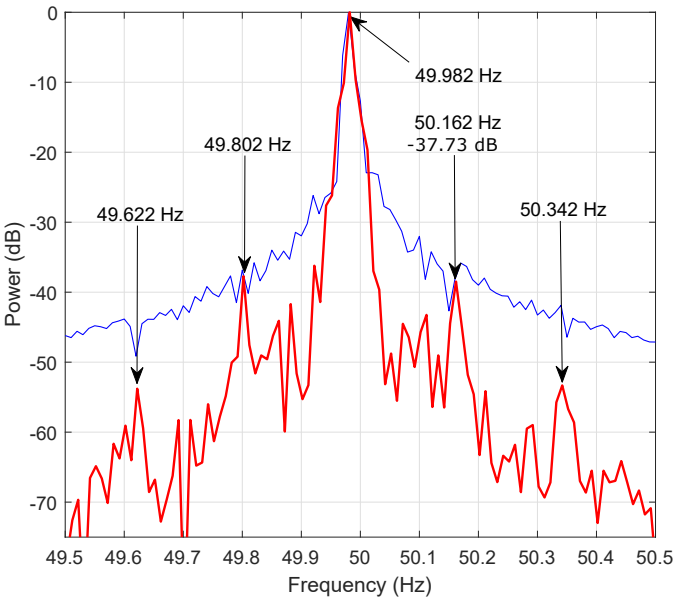

Fig. 13. Comparison between the conventional cDFT of the current of the faulty machine (thin, blue line), presented in Fig. 10, and the RLDFT obtained with the proposed method (thick, red line). The RLDFT practically avoids the leakage of the supply component, clearly shows the broken bar fault harmonics, and gives the supply frequency with milihertz precision.

It is worth mentioning that the current signal analyzed in this section has been obtained from a machine operating under real conditions, in an industrial process. As can be seen in the spectra presented in Fig. 10, Fig. 12 and Fig. 13 this signal contains multiple components apart from those related to the fault, caused by noise and the non-ideal character of

the machine. In this section the proper functioning of the proposed method has been verified despite the existence of these harmonic components, whose existence is unavoidable in actual machines operating in industrial environments.

A. *Comparison with the Classical FFT Approach*

In this section the RLDFT is compared with the classical FFT with weighting windows approach. First of all, the precise frequency of the supply component must be obtained via FFT interpolation, using the bin with the highest amplitude in the spectrogram and its adjacent bins (see Fig. 14, top).

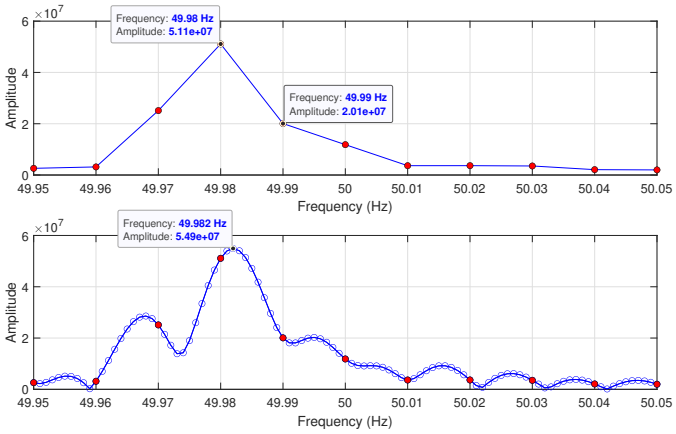

Fig. 14. Bins used for interpolating the actual value of the frequency supply, using the classical FFT (top), and its actual value read directly on the proposed fDFT (bottom), with a padding ratio $R_N = 10$. The filled red circles in both plots are the bins calculated with the classical FFT, and the hollow blue circles in the lower plot are the bins calculated with the zero-padded fDFT.

The interpolated value of the supply frequency is [15]

$$f_1 = 49.98 + \frac{2.01}{5.11 + 2.01}\frac{1}{100} = 49.9828 \text{ Hz} \qquad (36)$$

This value is more accurate than the frequency obtained with the classical FFT (49.98 Hz). It coincides with the frequency of the bin with the highest amplitude in the fDFT spectrum, Fig. 14, bottom ($f_{1\_app} = 49.982$ Hz). The same conclusion can be applied to the amplitude of the supply component.

The spectrum of the experimental current has been obtained using the classical FFT with two different weighting windows, the Hanning and the Chebyshev ones (see Fig. 15), and it has been compared with the RLDFT shown in Fig. 13. In both spectra, shown in Fig. 16 and Fig. 17, it can be observed that the RLDFT has a greater frequency resolvability, due to the lower width of the main lobe of the rectangular window, compared with the Hanning and Chebyshev windows (half and a quarter, respectively, as seen in Fig. 15). This is specially relevant around the principal fault harmonics, shown in a zoomed view in both figures. Moreover, the RLDFT achieves a greater leakage reduction than the classical FFT, and a higher precision in the frequencies of the main supply component and of the fault harmonics components.

About the required computing time, it takes 0.147 seconds to obtain the RDLFT, while it takes 0.013 seconds to obtain the classical FFT of the current with a weighting window, with the computer platform described in Appendix B. This increment in the computing time is due to the zero-padding of the current signal, which increases its length by a factor equal to the zero-padding ratio R_N.

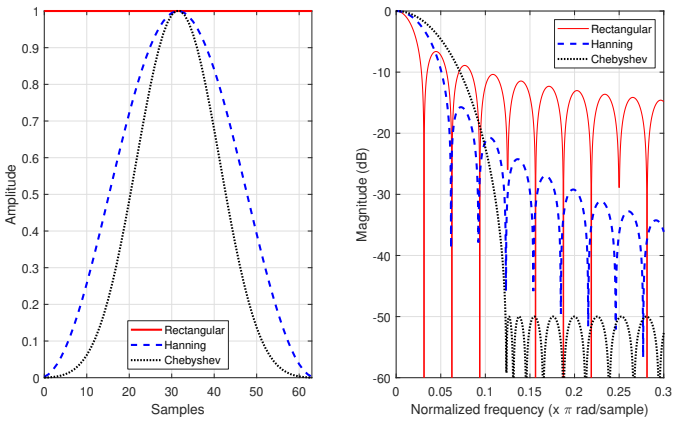

Fig. 15. Hanning and Chebyshev windows, in the time domain (left) and in the frequency domain (right), used for comparing the results of the RLDFT with the classical FFT approach.

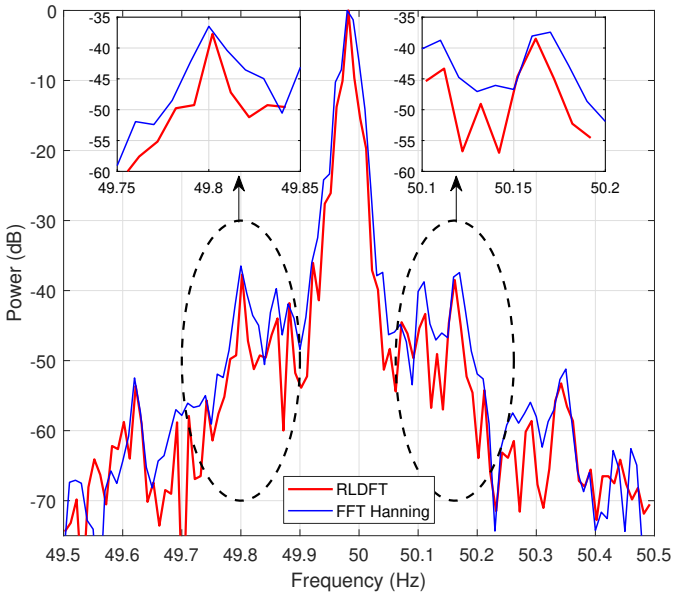

Fig. 16. Spectrogram of the current obtained with the RLDFT (red) and with a classical FFT with a Hanning weighting windows (blue). The RLDFT generates a sharper spectrogram, with well-defined peaks, especially around the fault harmonics (at 49.802 Hz and 50.162 Hz, zoomed top view), and with a lower spectral leakage.

VI. Conclusions

The leakage problem is one of the main obstacles for a reliable diagnosis of broken bar faults in large cage induction machines, working at very low slip. In this case, the fault harmonics are much smaller than the supply component and very close to it, so they are usually hidden under the spectral leakage in the conventional current spectrum. In this work, a new method for significantly reducing the spectral leakage of the supply component is proposed, thus improving the diagnostic reliability and avoiding misdiagnoses. It consists in obtaining a fine approximation to the CFT of the stator

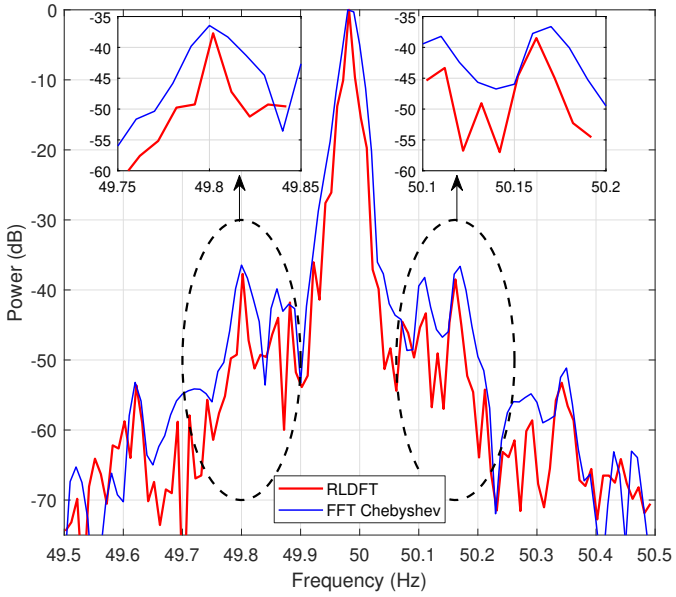

Fig. 17. Spectrogram of the current obtained with the RLDFT (red) and with a classical FFT with a Chebyshev weighting windows (blue). The RLDFT generates a sharper spectrogram, with well-defined peaks, especially around the fault harmonics (at 49.802 Hz and 50.162 Hz, zoomed top view), and with a lower spectral leakage.

current signal, the fDFT, by zero-padding the original sampled signal. In this fine spectrum, the position and amplitude of the supply component can be measured with a high precision. In a second step, using the fDFT bins where the leakage of the supply component is minimum, a reduced leakage conventional spectrum (RLDFT) is built, where the fault harmonics are clearly visible, even at extremely low slips. The method has been validated with the diagnosis of broken bars in a large cage induction motor.

APPENDIX A
RATED CHARACTERISTICS OF THE INDUCTION MACHINE

$P = 3.15$ MW, $f = 50$ Hz, $U = 6$ kV, $I = 373$ A, $n = 2982$ rpm, $\cos\varphi = 0.92$ and number of bars $= 56$.

APPENDIX B
COMPUTER FEATURES

CPU: Intel Core i7-2600K CPU @ 3.40 GHZ RAM memory: 16 GB, Matlab Version: 9.6.0.1072779 (R2019a).

REFERENCES

[1] S. Kumar, D. Mukherjee, P. K. Guchhait, R. Banerjee, A. K. Srivastava, D. N. Vishwakarma, and R. K. Saket, "A Comprehensive Review of Condition Based Prognostic Maintenance (CBPM) for Induction Motor," *IEEE Access*, vol. 7, pp. 90 690–90 704, 2019.

[2] F. B. Abid, M. Sallem, and A. Braham, "Robust Interpretable Deep Learning for Intelligent Fault Diagnosis of Induction Motors," *IEEE Trans. Instrum. Meas.*, vol. 69, no. 6, pp. 3506–3515, 2020.

[3] Z. Gao, C. Cecati, and S. X. Ding, "A Survey of Fault Diagnosis and Fault-Tolerant Techniques–Part I: Fault Diagnosis With Model-Based and Signal-Based Approaches," *IEEE Trans. Ind. Electron.*, vol. 62, no. 6, pp. 3757–3767, 2015.

[4] I. Culbert and J. Letal, "Signature Analysis for Online Motor Diagnostics: Early Detection of Rotating Machine Problems Prior to Failure," *IEEE Ind. Appl. Mag.*, vol. 23, no. 4, pp. 76–81, 2017.

[5] H. Li, G. Feng, D. Zhen, F. Gu, and A. D. Ball, "A Normalized Frequency Domain Energy Operator for Broken Rotor Bar Fault Diagnosis," *IEEE Trans. Instrum. Meas.*, vol. 70, pp. 1-10, 2021.

[6] S. T. Varghese, K. R. Rajagopal, and B. Singh, "Design and Development of Rotor Quality Test System for Die-Cast Copper Rotors," *IEEE Trans. Ind. Appl.*, vol. 54, no. 3, pp. 2105–2114, 2018.

[7] M. Drakaki, Y. L. Karnavas, A. D. Karlis, I. D. Chasiotis, and P. Tzionas, "Study on fault diagnosis of broken rotor bars in squirrel cage induction motors: a multi-agent system approach using intelligent classifiers," *IET Electric Power Applications*, vol. 14, no. 2, pp. 245–255, 2020.

[8] J. Burriel-Valencia, R. Puche-Panadero, J. Martinez-Roman, A. Sapena-Bano, and M. Pineda-Sanchez, "Fault Diagnosis of Induction Machines in a Transient Regime Using Current Sensors with an Optimized Slepian Window," *Sensors*, vol. 18, no. 2, p. 146, 2018.

[9] L. A. Trujillo-Guajardo, J. Rodriguez-Maldonado, M. A. Moonem, and M. A. Platas-Garza, "A Multiresolution Taylor-Kalman Approach for Broken Rotor Bar Detection in Cage Induction Motors," *IEEE Trans. Instrum. Meas.*, vol. 67, no. 6, pp. 1317 – 1328, 2018.

[10] R. Puche-Panadero, M. Pineda-Sanchez, M. Riera-Guasp, J. Roger-Folch, E. Hurtado-Perez, and J. Perez-Cruz, "Improved resolution of the MCSA method via Hilbert transform, enabling the diagnosis of rotor asymmetries at very low slip," *IEEE Trans. Energy Convers.*, vol. 24, no. 1, pp. 52–59, 2009.

[11] Y. Liu and A. M. Bazzi, "A review and comparison of fault detection and diagnosis methods for squirrel-cage induction motors: State of the art," *ISA Transactions*, vol. 70, pp. 400 – 409, 2017.

[12] G. Trejo-Caballero, H. Rostro-Gonzalez, R. D. J. Romero-Troncoso, C. H. Gerardo, Garcia-Capulin, O. G. Ibarra-Manzano, J. G. Avina-Cervantes, and A. Garcia-Perez, "Multiple signal classification based on automatic order selection method for broken rotor bar detection in induction motors," *Electr. Eng.*, vol. 99, no. 3, pp. 987–996, 2017.

[13] A. K. Samanta, A. Naha, A. Routray, and A. K. Deb, "Fast and accurate spectral estimation for online detection of partial broken bar in induction motors," *Mech. Syst. Signal Process.*, vol. 98, pp. 63–77, 2018.

[14] Y. Trachi, E. Elbouchikhi, V. Choqueuse, M. E. H. Benbouzid, and T. Wang, "A Novel Induction Machine Fault Detector Based on Hypothesis Testing," *IEEE Trans. Ind. Appl.*, vol. 53, no. 3, pp. 3039–3048, 2017.

[15] D. C. Rife and G. A. Vincent, "Use of the discrete Fourier transform in the measurement of frequencies and levels of tones," *Bell System Technical Journal*, vol. 49, no. 2, pp. 197–228, 1970.

[16] V. K. Jain, W. L. Collins, and D. C. Davis, "High-Accuracy Analog Measurements via Interpolated FFT," *IEEE Trans. Instrum. Meas.*, vol. 28, no. 2, pp. 113–122, 1979.

[17] D. Agrez, "Weighted multipoint interpolated DFT to improve amplitude estimation of multifrequency signal," *IEEE Trans. Instrum. Meas.*, vol. 51, no. 2, pp. 287–292, 2002.

[18] K. Wang, H. Wen, and G. Li, "Accurate Frequency Estimation by Using Three Points Interpolated DFT Based on Rectangular Window," *IEEE Trans. Industr. Inform.*, vol. 17, no. 1, pp. 73–81, 2021.

[19] D. Agrez, "Dynamics of Frequency Estimation in the Frequency Domain," *IEEE Trans. Instrum. Meas.*, vol. 56, no. 6, pp. 2111–2118, 2007.

[20] I. SANTAMARÍA, C. PANTALEÓN, and J. IBAÑEZ, "A COMPARATIVE STUDY OF HIGH-ACCURACY FREQUENCY ESTIMATION METHODS," *Mechanical Systems and Signal Processing*, vol. 14, no. 5, pp. 819–834, 2000.

[21] S. Rapuano and F. Harris, "An introduction to FFT and time domain windows," *IEEE Instrumentation & Measurement Magazine*, vol. 10, no. 6, pp. 32–44, 2007.

[22] R. Hidalgo, J. Fernandez, R. Rivera, and H. Larrondo, "A simple adjustable window algorithm to improve FFT measurements," *IEEE Trans. Instrum. Meas.*, vol. 51, no. 1, pp. 31–36, 2002.

[23] A. Sapena-Bano, M. Pineda-Sanchez, R. Puche-Panadero, J. Perez-Cruz, J. Roger-Folch, M. Riera-Guasp, and J. Martinez-Roman, "Harmonic Order Tracking Analysis: A Novel Method for Fault Diagnosis in Induction Machines," *IEEE Trans. Energy Convers.*, vol. 30, no. 3, pp. 833–841, 2015.

[24] K. F. Chen and S. L. Mei, "Composite Interpolated Fast Fourier Transform With the Hanning Window," *IEEE Trans. Instrum. Meas.*, vol. 59, no. 6, pp. 1571–1579, 2010.

[25] M. Mottaghi-Kashtiban and M. Shayesteh, "New efficient window function replacement for the Hamming window," *IET Signal Processing*, vol. 5, no. 5, p. 499, 2011.

[26] T. A. Garcia-Calva, D. Morinigo-Sotelo, A. Garcia-Perez, D. Camarena-Martinez, and R. de Jesus Romero-Troncoso, "Demodulation Technique for Broken Rotor Bar Detection in Inverter-Fed Induction Motor Under

Non-Stationary Conditions," *IEEE Trans. Energy Convers.*, vol. 34, no. 3, pp. 1496–1503, 2019.

[27] F. F. Costa, L. A. L. de Almeida, S. R. Naidu, and E. R. Braga-Filho, "Improving the signal data acquisition in condition monitoring of electrical machines," *IEEE Trans. Instrum. Meas.*, vol. 53, no. 4, pp. 1015–1019, 2004.

[28] A. Naha, S. Member, A. K. Samanta, and S. Member, "A Method for Detecting Half-Broken Rotor Bar in Lightly Loaded Induction Motors Using Current," *IEEE Trans. Instrum. Meas.*, vol. 65, no. 7, pp. 1614–1625, 2016.

[29] R. Puche-Panadero, J. Martinez-Roman, A. Sapena-Bano, and J. Burriel-Valencia, "Diagnosis of Rotor Asymmetries Faults in Induction Machines Using the Rectified Stator Current," *IEEE Trans. Energy Convers.*, vol. 35, no. 1, pp. 213–221, 2020.